J Math Chem (2009) 45:7–38
DOI 10.1007/s10910-008-9364-9

ORIGINAL PAPER

Thoughts on lattice knot statistics

E. J. Janse van Rensburg

Received: 15 June 2007 / Accepted: 21 November 2007 / Published online: 27 August 2008

Abstract Lattice knot statistics, or the study of knotted polygons in the cubic lattice, gained momentum in 1988 when the Frisch-Wasserman-Delbruck conjecture was proven by Sumners and Whittington (J Phys A Math Gen 21:L857–861, 1988), and independently in 1989 by Pippenger (Disc Appl Math 25:273–278, 1989). In this paper, aspects of lattice knot statistics are reviewed. The basic ideas underlying the study of knotted lattice polygons are presented, and the many open problem are posed explicitly. In addition, the properties of knotted polygons in a confining slab geometry are explained, as well as the Monte Carlo simulation of knotted polygons in $\mathbb{Z}^3$ and in a slab geometry. Finally, the mean behaviour of lattice knots in a slab are discussed as a function of the knot type.

Keywords Lattice knots · Ring polymer · Connective constant · Statistical topology

1 Introduction

Lattice knot statistics was boosted to prominence in the late 1980's when the Frisch-Wasserman-Delbruck conjecture [6, 7] was settled in the cubic lattice almost thirty years after it was made, by Sumners and Whittington [36] and by Pippenger [32]. This conjecture, made in the context of knotting in ring polymers, implies that the probability that a polymer in a good solvent is knotted approaches one as the length of the polymer is increased.

This result inspired activity in the field, with the extension of the Frisch-Wasserman-Delbruck conjecture to interacting polygons (for an example, see Ref. [15]), the study of the statistical geometric properties of lattice knots in the form of writhing and

E. J. Janse van Rensburg (✉)
Department of Mathematics and Statistics, York University, Toronto, ON, Canada M3J 1P3
e-mail: rensburg@yorku.ca

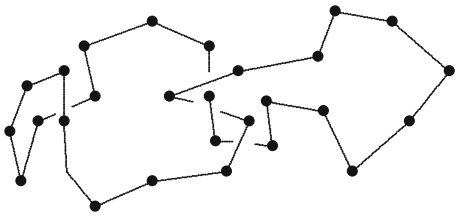

Fig. 1 A bond-stick polygon model of a polymer in three space. This particular example is a non-trivial knotted polygon which cannot be continuously deformed into the unknot without passing through conformations with singular points (or self-intersections)

twisting [14, 30, 37], and the development of algorithms for the Monte Carlo sampling of lattice knots and the numerical study of knotting and of knot statistics in the cubic lattice [11, 16, 17].

The normal mathematical model for a ring polymer is a polygon as illustrated in Fig. 1. The simplest version of these models are uniformly weighted polygons in three space, and the free energy in such a model depends only on entropic contributions arising from the conformational degrees of freedom. Such models are considered to model ring polymers in a good solvent [5].

A particularly interesting and rich polygon model of a ring polymer is a *lattice polygon*, consisting of the placement of a polygon in a lattice, usually the two dimensional square lattice, or the three dimensional cubic lattice. This model is amenable to both numerical treatment in the form of Monte Carlo simulations, and to rigorous treatment. A large and active field of study have grown around lattice polygons, including the development of algorithms for Monte Carlo simulations, the development of scaling arguments for understanding scaling and critical behaviour in these models, and also the application of rigorous mathematical arguments to prove the existence of scaling limits and critical points, and to study the role of conformational degrees of freedom in the free energy. The Frisch-Wasserman-Delbruck conjecture was settled in the mathematical context for cubic lattice polygons [32, 36].

The polygon model of a ring polymer in three space illustrated in Fig. 1 is self-avoiding. Since the polygon is itself composed of thin one dimensional edges, this self-avoidance has little effect on its entropic properties. In this context a lattice model with excluded volume (self-avoidance) is a more realistic model of a ring polymer: each vertex in a lattice polygon excludes a cubical volume of unit side length centered at the vertex, and this has a dramatic effect on the mathematical properties of the model.

The self-avoiding walk is the archetypical polymer model with excluded volume [9]. The non-Markovian nature of this model gives a rich mathematical structure, and the subject of intensive research from a variety of different points of view [25]. A (self-avoiding) polygon in the cubic lattice is composed of unit length edges and a self-avoiding, see Fig. 2 for an example in the square lattice.

In three dimensions a lattice polygon is a model of a three dimensional ring polymer. Such lattice polygons are often called *lattice knots*. These are special cases of lattice polygons, and the topological properties of the polygons are of critical concern in these models.

In a lattice polygon model of a ring polymer, two polygons are considered to be equivalent if one can be translated upon the other. Define p_n to be the number of

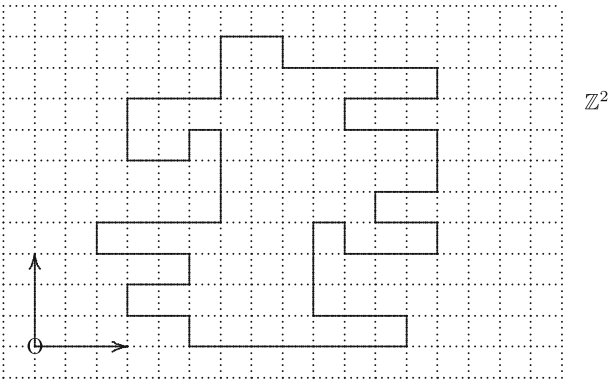

Fig. 2 A square lattice polygon model of a ring polymer in a good solvent. The excluded volume effect in lattice polygons has an important effect on the statistical properties of the model

equivalence classes of polygons, counted up to translational equivalence. This quantity is the most fundamental in a lattice polygon model.

It is relatively easy to check that in the square lattice, $p_4 = 1$, $p_6 = 2$ and $p_8 = 7$, but p_n increases exponentially with n, and it soon becomes a tremendous challenge to enumerate it for increasing values of n. Currently, p_n is known for (even) $n \leq 110$ [19] in the square lattice, and the series in higher dimensions are much shorter. The (intensive) free energy in this model is composed purely of entropic terms and is defined by $(\log p_n)/n$.

The *growth constant* μ is defined by

$$\mu = \lim_{n\to\infty} p_n^{1/n} \tag{1}$$

and gives the (exponential) rate at which p_n is growing. The existence of this limit is known (see Sect. 2).

A "grand canonical" version of this model is obtained if a monomer activity t associated with the number of monomers is introduced. This gives rise to a generating function description of polygons in the lattice, where the radius of convergence t_c of the generating function

$$g(t) = \sum_{n>0} p_n t^n \tag{2}$$

can be analysed to gain information on the limiting value of the free energy as $n \to \infty$: it follows that $t_c^{-1} = \lim_{n\to\infty}[(\log p_n)/n] = \log \mu$. This ensemble is somewhat unphysical in the sense that it models a ring polymer sampled from a distribution of different lengths at a "monomer activity" t, and with expected values (mean length, knotting properties, size, etc.) over the entire (Boltzman) ensemble. In spite of this, it is still possible to gain useful information on the statistical properties of polygons by analysing polygons in this ensemble.

In this paper a review of the basic properties of polygons and of lattice knots in the cubic lattice is given. This review is not meant to be comprehensive, but will instead focus on some fairly narrow issues concerned with the statistical properties of lattice knots, with the simulation of lattice knots, and with the properties of lattice knots in a slab (this is a model of a knotted ring polymer in a confining geometry).

In general the presence of a knot in a polygon has an effect on its conformational entropy, and therefore on other properties of the polygon, such as its size. In Sect. 2 I review the most basic results in the study of lattice knots. The properties of the generating function of polygons, and of lattice knots, are briefly presented and reviewed. There are numerous open problems, and some of these are posed explicitly.

In Sect. 3 attention is given to lattice polygons in a slab. This is a model of a ring polymer in a confined geometry. If $p_n(w)$ is the number of polygons of length n in a slab of width w, then the limit $\lim_{n\to\infty}(p_n(w))^{1/n} = \mu_w$ [35] gives the growth constant of $p_n(w)$. It is known that $\mu_w \to \mu$ as $w \to \infty$ [15], and the rate at which $\mu_w \to \mu$ can be obtained by using a scaling argument.

Next, attention is turned to knotted polygons in a slab of width w. If $p_n(K; w)$ is the number of lattice polygons of knot type K, in a slab of width w and of length n, then the generating function is

$$g_{K,w}(t) = \sum_{n>0} p_n(K, w)t^n. \tag{3}$$

In this ensemble a scaling argument can be used to predict the expected length of polygons. This is given by

$$\langle n\rangle_{K,w} = \frac{d\ \log g_{K,w}(t)}{d\log t} = \frac{\sum_{n>0} n\ p_n(K, w)t^n}{\sum_{n>0} p_n(K, w)t^n}. \tag{4}$$

At the critical point $t = 1/\mu_\emptyset$ of the generating function of unknotted polygons $\langle n\rangle_{K,w}$ is shown to approach a constant as $w \to \infty$ if K is the unknot, while $\langle n\rangle_{K,w}$ diverges with increasing w if K is a non-trivial knot. A scaling argument also indicates that if K is a prime knot, then $\langle n\rangle_{K,w}$ diverges along a concave curve, while if K is a compound knot, then $\langle n\rangle_{K,w}$ diverges along a convex curve [13].

In Sect. 4 the BFACF algorithm for sampling lattice knots along a Markov Chain is reviewed. This algorithm is known to have ergodicity classes in $\mathbb{Z}^3$ which coincides with the knot types of the lattice polygons [17]. In a slab of width $w > 1$ this algorithm is also known to have ergodicity classes coinciding with lattice knot types [13]. In Sect. 5 I review data obtained by sampling lattice knots in $\mathbb{Z}^3$ and in slabs of widths $w \in [0, 20]$. In particular, the algorithm was used to collect data on $\langle n\rangle_{K,w}$ for a set of knots and to examine the predictions of scaling arguments. Results on the growth constant, the entropic exponents, the metric exponent, and the mean length, and amplitude ratios of lattice knots confined to a slab are also reviewed in Sect. 5.

In Sect. 6 a few short final conclusions are made.

2 Lattice polygons, and knotted lattice polygons

2.1 Lattice polygons: a short review

Consider the hypercubic lattice $\mathbb{Z}^d$ and let the coordinates of a vertex $x \in \mathbb{Z}^d$ be denoted by $(X(x), Y(x), \ldots, Z(x))$, with $X(x)$ denoting the first coordinate, and $Z(x)$ always denoting the last coordinate.

We define the *bottom vertex* of a polygon to be its lexicographic least vertex, and its *top vertex* to be its lexicographic most vertex. Incident with the bottom vertex of a polygon are two edges, one of which has lexicographic least midpoint, and which is normal to the X-direction. This is the *bottom edge* of the polygon. Similarly, incident with the top vertex of a polygon are two edges, one of which has lexicographic most midpoint and which is normal to the X-direction. This is the *top edge* of the polygon.

Two polygons in $\mathbb{Z}^d$ can be concatenated by translating and rotating the second polygon until its bottom edge is parallel to the top edge of the first polygon (see Fig. 3) and with first coordinate bigger by one. By deleting these top and bottom edges, and inserting two edges to reconnect the two polygons into a single polygon, the polygons are concatenated. If the first and second polygons had lengths n and m, then there were p_n choices for the first polygon, and $p_m/(d-1)$ choices for the second, and the number of distinct polygons of lengths $n+m$ which can be obtained in this construction is at most p_{n+m}. Thus,

$$p_n\, p_m/(d-1) \leq p_{n+m}. \tag{5}$$

By applying Fekete's lemma to this supermultiplicative inequality [8], the result is that the limit

$$\lim_{n\to\infty} p_n^{1/n} = \mu \tag{6}$$

exists. The *growth constant* μ determines the exponential rate at which p_n increases with n. In particular, since $p_n \leq (2d)^n$, μ is finite, and existence of the above limit implies that $p_n = \mu^{n+o(n)}$ and $p_n \leq (d-1)\mu^n$. Observe as well that $p_n \geq 2^{n/2}$ so that $\mu \geq \sqrt{2}$.

In the three dimensional (cubic) lattice the growth constant μ has been estimated from self-avoiding walk enumeration using lace expansions [10] in Ref. [4]. The best

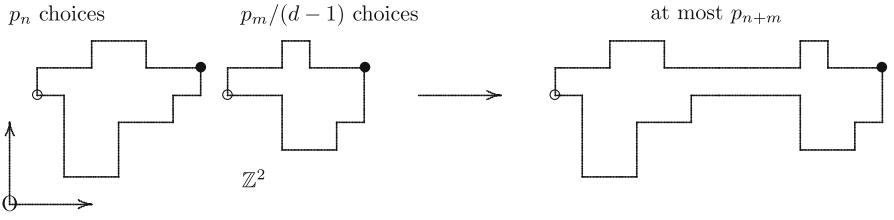

Fig. 3 Concatenating two polygons in the hypercubic lattice. Bottom vertices are donoted by ○'s, and top vertices are denoted by ●'s

estimate is

$$\mu = 4.684043 \pm 0.000012. \tag{7}$$

This follows since polygons and self-avoiding walks can be shown to have the same growth constant [8].

The *pattern theorem* for lattice polygons may be stated as follows: A *pattern* is any finite length self-avoiding walk. A pattern P is said to *occur* in a polygon if P is identical, up to translation, with a sub-walk in the polygon. A pattern P is *proper* if it can occur three times in a self-avoiding walk. Let $p_n(\leq \lfloor \epsilon n \rfloor\, P)$ be the number of lattice polygons of length n, with at most $\lfloor \epsilon n \rfloor$ occurrences of the proper pattern P. The pattern theorem states that for any proper pattern P there is an $\epsilon > 0$ such that

$$\limsup_{n\to\infty} \left(p_n(\leq \lfloor \epsilon n \rfloor\, P)\right)^{1/n} < \mu. \tag{8}$$

In other words, the set of polygons which contains at least $\lfloor \epsilon n \rfloor$ occurrences of P, with cardinality $p_n - p_n(\leq \lfloor \epsilon n \rfloor\, P)$, grows at the same exponential rate as p_n itself. This result for polygons is based on a pattern theorem for self-avoiding walks [20, 21] (see [12] for a proof for polygons using a method due to D J A Welsh). The pattern theorem for polygons was used to prove the Frisch-Wasserman-Delbruck conjecture [32, 36].

These are the most important rigorous results in low dimensions for lattice polygons—most other results are in one way or another based on these. A theoretical (but not rigorous) interpretation of polygons as arising in the $N \to 0$ limit of a $O(N)$ model [28] suggests the asymptotic form

$$p_n = A\, n^{\alpha-3} \mu^n \left(1 + B\, n^{-\Delta} + C\, n^{-1} + \cdots\right) \tag{9}$$

for p_n, with a powerlaw correction to the pure exponential growth term where α is often called the *entropic* or *specific heat* exponent. Corrections to this are both analytic (as in the terms $C\, n^{-1}$) and non-analytic (as in the terms $B\, n^{-\Delta}$), where the confluent correction exponent Δ is the first in a hierarchy of higher order corrections. For the (numerical) purposes here, the corrections will be ignored, and the assumption that $p_n \approx A\, n^{\alpha-3} \mu^n$ could be made. It is known that $\alpha - 3 < -1$ in three dimensions [23, 24]. Thus, the generating function defined in Eq. 2 is finite at its radius of convergence, which is given by $t_c = 1/\mu$ by Eq. 6. Simulations have shown that $\alpha = 0.237 \pm 0.005$ and $\Delta = 0.56 \pm 0.03$ [22].

The generating function of lattice polygons with an activity t conjugate to the number of vertices is defined by Eq. 2. Observe that the singular behaviour of $g(t)$ suggested by Eq. 9 is given by

$$g(t) \sim |\log(\mu t)|^{2-\alpha}, \tag{10}$$

and this is only be singular part in $g(t)$. The critical point in $g(t)$ is at $t = 1/\mu$, and since $\alpha - 3 < -1$ [24], $g(1/\mu)$ is finite. Hence,

$$g(t) \approx g(1/\mu)\left(1 - C\,|\log(\mu t)|^{2-\alpha}\right) \tag{11}$$

as $t \to 1/\mu$ from below.

The average length of polygons in this (grand canonical) ensemble (with $g(t)$ playing the role of a grand partition function) is given by

$$\langle n\rangle = \frac{d}{d\log t}\log g(t) \approx \text{Const.} + \frac{C(2-\alpha)|\log(t\mu)|^{1-\alpha}}{1 - C\,|\log(t\mu)|^{2-\alpha}}. \tag{12}$$

Since $p_n = \mu^{n+o(n)}$, the radius of convergence of $g(t)$ is given by $t = 1/\mu$, and by putting $t = 1/\mu$ in the above, one obtains the result that

$$\langle n\rangle|_{t=1/\mu} = \text{Const.} \tag{13}$$

In other words, the expected length of polygons at the critical value of $t{=}1/\mu$ is finite.

2.2 Knotted lattice polygons

A polygon is a piecewise linear embedding of a circle into $\mathbb{Z}^3$ and thus into three space, see Fig. 4. The knot type K of a given polygon is therefore well defined. Define $p_n(K)$ to be the number of lattice polygons of length n and of knot type K, counted up to equivalence under translations in the cubic lattice. Concatenation of two polygons of knot types K and L can still be done as illustrated in Fig. 3, and the result is a polygon with compound knot type $K\#L$. In particular, this implies that

$$p_n(K)\,p_m(L) \le p_{n+m}(K\#L). \tag{14}$$

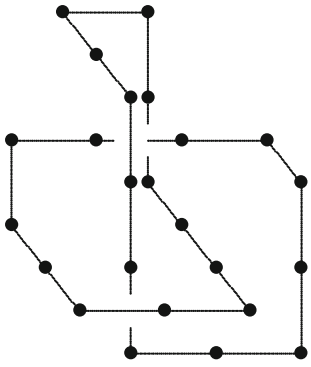

Fig. 4 A knotted lattice polygon with 24 steps in the cubic lattice

If $K = L = \emptyset$, where $\emptyset$ denote the unknot, then this shows that

$$p_n(\emptyset)\, p_m(\emptyset) \leq p_{n+m}(\emptyset) \tag{15}$$

with the result that the limit

$$\lim_{n\to\infty} [p_n(\emptyset)]^{1/n} = \mu_\emptyset \tag{16}$$

exists, where $\mu_\emptyset$ is the growth constant of unknotted lattice polygons.

The Frisch-Wasserman-Delbruck conjecture implied that $\mu_\emptyset < \mu$. Numerical simulations [16, 38] indicate that

$$\log \mu - \log \mu_\emptyset = (4.15 \pm 0.32) \times 10^{-6}. \tag{17}$$

In other words, $\mu = 4.6841\ldots$ and $\mu_\emptyset = 4.6841\ldots$, and there is a difference in the next one or two digits. Current computational technology could determine the next couple of digits in μ and $\mu_\emptyset$ (while μ is known at least to the accuracy in Eq. 7), but this remains a tremendous computational challenge. The next digits in these growth constants is stated as an open problem:

Open problem 2.1 *Determine, by Monte Carlo simulation, series enumeration or otherwise, the next digits in μ and in $\mu_\emptyset$, by improving the estimates in Eqs. 7 and 17.*

The existence of $\mu_\emptyset$ as a limit in Eq. 16 is a special case. For non-trivial knot types, it is not known that a similar limit exists. Instead one defines the limsup

$$\mu_K = \limsup_{n\to\infty} [p_n(K)]^{1/n}. \tag{18}$$

The existence of μ_K as a limit is a major open problem in the study of lattice knots.

Open problem 2.2 *Prove that the limit*

$$\mu_K = \lim_{n\to\infty} [p_n(K)]^{1/n}$$

exists for arbitrary and fixed non-trivial knot types K.

It is known that [34]

$$\mu_\emptyset \leq \mu_K < \mu. \tag{19}$$

Settling the first inequality is yet another open problem. Generally, it is accepted that this should be an equality.

Open problem 2.3 *Prove that $\mu_\emptyset = \mu_K$ for arbitrary and fixed non-trivial knot types K.*

A pattern theorem is not known for polygons of fixed knot types. In particular, it seems that one should be able to prove such a theorem for the case of unknotted polygons. This is yet another open problem.

Open problem 2.4 *Prove a pattern theorem for unknotted polygons in the cubic lattice.*

More generally, one could hope for a more general theorem:

Open problem 2.5 *Prove a pattern theorem for lattice polygons of fixed knot type K in the cubic lattice.*

Apart from settling the Frisch-Wasserman-Delbruck conjecture, little progress has been made understanding the statistical properties of knotted lattice polygons. Generally, this is a field that is known more for its basic open problems, rather than for its theorems.

In analogy with p_n, it is generally expected that the asymptotic form for $p_n(K)$ should be

$$p_n(K) = A_K n^{\alpha_K - 3} \mu_K^n (1 + B_K n^{-\Delta_K} + C_K n^{-1} + \cdots). \tag{20}$$

There is tremendous numerical support for this assumption. Numerical simulations in Ref. [31] suggest that $\mu_K = \mu_\emptyset$ and also the rather surprising fact that A_K is independent of K (if the assumption that $\mu_\emptyset = \mu_K$ is made). The entropic exponent of lattice knots, α_K, appears to be related to the entropic exponent $\alpha_\emptyset$ of unknotted polygons by

$$\alpha_K = \alpha_\emptyset + N_K \tag{21}$$

where N_K is the number of prime components in the knot type K. For example, $\alpha_{3_1} = \alpha_\emptyset + 1$, while $\alpha_{3_1 \# 3_1} = \alpha_\emptyset + 2$. However, unlike p_n, the asymptotic formula for $p_n(K)$ in Eq. 20 does not rest on a theoretical foundation such as an $O(N)$ model. Settling this is unlikely to be a rigorous result, but this remains an open problem.

Open problem 2.6 *If K is a fixed knot type, show that the asymptotic formula*

$$p_n(K) = A_K n^{\alpha_K - 3} \mu_K^n (1 + B_K n^{-\Delta_K} + C_K n^{-1} + \cdots)$$

can be obtained from a (non-rigorous) field theoretic argument. Show this in particular for $K = \emptyset$. In addition, provide theoretical support for the relation

$$\alpha_K = \alpha_\emptyset + N_K$$

amongst the entropic exponents of lattice knots of fixed knot type.

These open problems have been tested numerically, see for example Refs. [29, 31].

3 Polygons in confined spaces: slabs in the cubic lattice

A *slab* of width w, denoted by $\mathbb{L}_w$, is the space

$$\mathbb{L}_w = \{x \in \mathbb{Z}^d \,|\, 0 \leq Z(x) \leq w\}. \tag{22}$$

A polygon ω is confined to $\mathbb{L}_w$ if each vertex in ω is contained in $\mathbb{L}_w$. The plane $Z = 0$ is the *bottom bounding plane* of $\mathbb{L}_w$, and $Z = w$ is the *top bounding plane* of $\mathbb{L}_w$.

A polygon in a slab is a model of a ring polymer in a confined space, see Fig. 5. In the grand canonical version of this model, there is an activity t associated with each monomer or vertex, and the polygon maintains a mean length which depends on the width w of the slab.

In the square or cubic lattice the model becomes a lattice polygon confined to a slab $\mathbb{L}_w$ (see Fig. 6). Define $p_n(w)$ to be the number of polygons of length n in a slab $\mathbb{L}_w$ of width w, counted up to equivalence under translations parallel to the bounding planes of the slab. The *Z-span* or *span* of a polygon ω in $\mathbb{L}_w$ is defined by

$$S_z(\omega) = \max_{x,y\in\omega} |Z(x) - Z(y)|\,. \tag{23}$$

Two polygons in a slab $\mathbb{L}_w$ can be concatenated as illustrated in Fig. 7. A narrow polygon τ of span w is placed in $\mathbb{L}_w$ between the two polygons, which are then each concatenated to τ. Details of the construction depends on the number of dimensions,

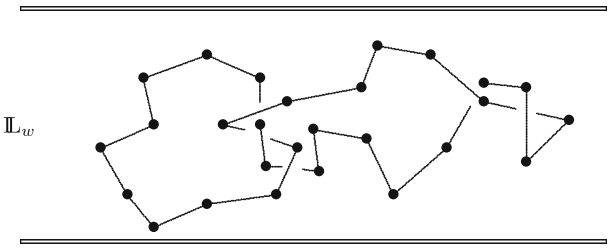

Fig. 5 A polygon in a slab $\mathbb{L}_w$ is a model of a ring polymer in a confined space. Narrowing the slab reduces the conformational entropy of the polygon, resulting in a (repulsive) entropic force being exerted on the walls of the slab. In this example, the polygon is a knot

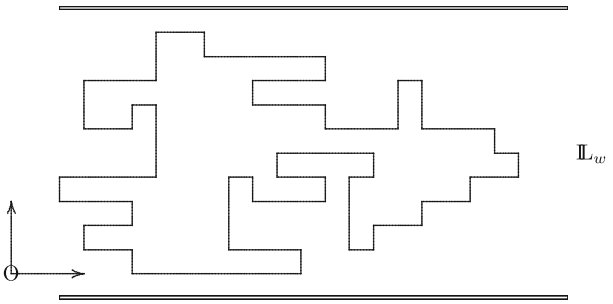

Fig. 6 A lattice polygon model of a ring polymer in a slab geometry

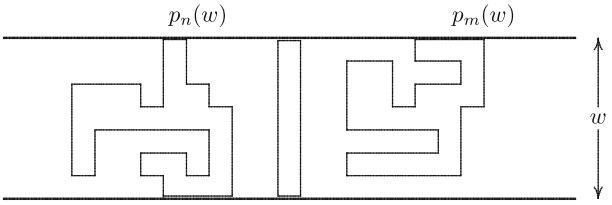

Fig. 7 Concatenating two polygons, the first of length n and the second of length m, in a slab $\mathbb{L}_w$. A polygon of Z-span w and length $2w + 1$ is inserted in the slab, and the first polygon is translated to its left-side, while the second is translated to its right side. The construction is performed by removing and adding edges to join these polygons up into a single polygon of length $n + m + 2w + 1$

and is easier in two dimensions, see Refs. [35, 39], and Ref. [40] for related results. The result is the supermultiplicative inequality

$$p_n(w)p_m(w) \leq p_{n+m+k}(w) \tag{24}$$

where k is a constant (and $k = 2(w + 1)$ in two dimensions). Since $p_n(w) \leq p_n$, the result is the existence of a growth constant in this model:

$$\lim_{n\to\infty} p_n^{1/n}(w) = \mu_w. \tag{25}$$

The free energy $\mathcal{F}(w)$ in this model is defined in the usual way by

$$F_n(w) = \frac{1}{n} \log p_n(w) \tag{26}$$

and it is known that $F_n(w) \to \log \mu_w$ as $n \to \infty$ [15], and the limiting free energy is defined by

$$\mathcal{F}(w) = \log \mu_w. \tag{27}$$

It is generally believed, in analogy with Eq. 9, that $p_n(w)$ has asymptotic behaviour given by

$$p_n(w) = A_w n^{\alpha_w - 3} \mu_w^n \left(1 + B_w n^{-\Delta_w} + C_w n^{-1} + \cdots\right). \tag{28}$$

It is known that $\mu_w \to \mu$ as $w \to \infty$:

Theorem 3.1 *It is the case that* $\mu_w < \mu_{w+1} < \mu$ *for finite* w, *and*

$$\lim_{w\to\infty} \mu_w = \mu.$$

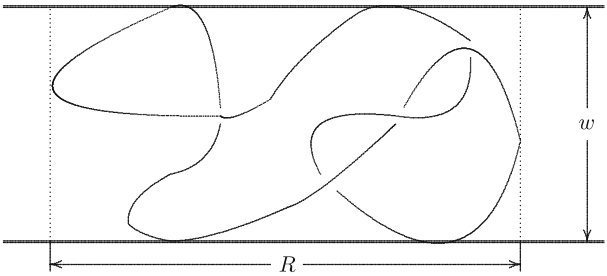

Fig. 8 A schematic diagram of a lattice polygon in a slab of width w. There are two length scales in this model, namely the width w of the slab, and the size R of the polygon. The (intensive) free energy is a function of the ratio R/w

For a proof of this theorem, see Ref. [15].

The relationship between μ_w and μ can be further examined by using a scaling argument. In Fig. 8 a schematic diagram of a polygon in a slab of width w is given. There are two length scales in this model, namely the width w of the slab, and the size R of the polygon. The size of the polygon in the lattice scales with its length n as $R \sim n^{\nu}$ where ν is the *metric exponent*.

The free energy in this model is an intensive quantity, and it is a function of the ratio of the length scales:

$$\mathcal{F}_w = n^{-1} F(R/w) = w^{-1/\nu} F_1(n^{\nu}/w). \tag{29}$$

Since $\mathcal{F}_w = \log \mu_w$, this together with Theorem 3.1 implies that for constant n^{ν}/w,

$$\mu_w \sim \mu\, e^{-C\, w^{-1/\nu}} \approx \mu(1 - C\, w^{-1/\nu}) \tag{30}$$

for some unknown constant C.

The generating function in this model is given by

$$g_w(t) = \sum_{n>0} p_n(w) t^n \tag{31}$$

at activity t. Using the asymptotic form for $p_n(w)$ in Eq. 28 then suggest that the singular part of $g_w(t)$ have approximate behaviour given by

$$g_w(t) \sim |\log(\mu_w t)|^{2-\alpha_w} \tag{32}$$

and this gives the rate at which $g_w(t)$ approaches $g_\infty(t)$ as $w \to \infty$:

$$g_w(t) \approx g_\infty(t) \left(1 - C\, |\log(\mu_w t)|^{2-\alpha_w}\right). \tag{33}$$

Since $\mu_w < \mu$, the singularity in $g_w(t)$ is approached when $t \to 1/\mu_w$. Putting $t = 1/\mu < 1/\mu_w$ in Eq. 33, and comparing it to Eq. 11 then indicates that

$g_\infty(1/\mu) \le g(1/\mu) < \infty$, and one may compute the average length of polygons in a slab of width w at activity $t_c = 1/\mu$. This is done exactly as in Eq. 12, in this case by exploiting the assumption in Eq. 28; the result is

$$\langle n \rangle_w = \frac{d}{d \log t} \log g_w(t) \approx \text{Const.} + \frac{C(2-\alpha_w)|\log(t\mu_w)|^{1-\alpha_w}}{1 - C\,|\log(t\mu_w)|^{2-\alpha_w}}. \tag{34}$$

Putting $t = 1/\mu$ gives the average length at the critical point in the slab $\mathbb{L}_w$ of width w:

$$\langle n \rangle_w \approx \text{Const.} + \frac{C(2-\alpha_w)|\log(\mu_w/\mu)|^{1-\alpha_w}}{1 - C\,|\log(\mu_w/\mu)|^{2-\alpha_w}}. \tag{35}$$

Finally, noting the relationship between μ and μ_w in Eq. 30 gives to leading order

$$\langle n \rangle_w \approx \text{Const.} + C_1 w^{-(1-\alpha_w)/\nu} + \cdots. \tag{36}$$

This relation, derived from a scaling argument, and using the relationship between μ and μ_w, gives the dependence of the expected length of a polygon in a slab of width w when $t = 1/\mu$.

3.1 Knotted polygons in a slab

In the case that a lattice knot in the slab $\mathbb{L}_w$ is examined, a similar argument is used. Define $p_n(K, w)$ to be the number of lattice knots of knot type K and length n in the slab $\mathbb{L}_w$ of width w, and counting up to equivalence under translations parallel to the bottom bounding place of $\mathbb{L}_w$.

The basic assumption that

$$p_n(K, w) = A_{K,w} n^{\alpha_{K,w}-3} \mu_{K,w}^n \left(1 + B_{K,w} n^{-\Delta_{K,w}} + C_{K,w} n^{-1} + \cdots\right) \tag{37}$$

is made in analogy with Eq. 20. This poses another open problem.

Open problem 3.2 *Prove that $p_n(K, w) = \mu_{K,w}^{n+o(n)}$, were $\mu_{K,w} = \mu_{\emptyset,w}$ is independent of K. This implies that the limit*

$$\lim_{n\to\infty} \frac{1}{n} \log p_n(K, w) = \log \mu_{\emptyset,w}$$

exists and is independent of K.

Additionally, it is expected that the relationship between α_K and $\alpha_\emptyset$ in Eq. 21 is maintained in $\mathbb{L}_w$:

$$\alpha_{K,w} = \alpha_{\emptyset,w} + N_K. \tag{38}$$

Demonstrating that this is true is an open problem.

Open problem 3.3 *If K is a fixed knot type, show that the asymptotic formula*

$$p_n(K, w) = A_{K,w} n^{\alpha_{K,w}-3} \mu_{\emptyset,w}^n (1 + B_{K,w} n^{-\Delta_{K,w}} + C_{K,w} n^{-1} + \cdots)$$

can be obtained from a (non-rigorous) field theoretic argument. Show this in particular for $K = \emptyset$. In addition, provide theoretical support for the relation

$$\alpha_{K,w} = \alpha_{\emptyset,w} + N_K$$

amongst the entropic exponents of lattice knots of fixed knot type in a slab $\mathbb{L}_w$. In addition, show that $\alpha_{\emptyset,w} = \alpha_w$.

Assume that the relationship between α_K and $\alpha_\emptyset$ in Eq. 21 is maintained in $\mathbb{L}_w$: $\alpha_{K,w} = \alpha_{\emptyset,w} + N_K$. With these assumptions, the expected length of knotted polygons in a slab $\mathbb{L}_w$ at $t = 1/\mu$ can be estimated in the same way as above. The result is

$$\langle n \rangle_{K,w} \approx \text{Const.} + \frac{C(2 - \alpha_{K,w}) |\log(\mu_w/\mu)|^{1-\alpha_{K,w}}}{1 - C\,|\log(\mu_w/\mu)|^{2-\alpha_{K,w}}}. \tag{39}$$

Substituting $\alpha_{K,w} = \alpha_{\emptyset,w} + N_K$ in this, and assuming that $\alpha_{\emptyset,w} < 1$, then gives the following leading order dependences for $\langle n \rangle_{K,w}$:

$$\langle n \rangle_{K,w} = \begin{cases} C_1 + O(w^{-(1-\alpha_{\emptyset,w})/\nu}) & \text{for unknots,} \\ C_2 + O(w^{\alpha_{\emptyset,w}/\nu}) & \text{for prime knots,} \\ C_3 + O(w^{1/\nu}) & \text{for compound knots.} \end{cases} \tag{40}$$

Assuming that $\alpha_{\emptyset,w} \approx 1/2$ (this is close to its two dimensional value since $\mathbb{L}_w$ is almost two dimensional in the scaling limit), and assuming that $\nu = 0.588$ (this is close to the numerical value for ν [22]), then gives

$$\langle n \rangle_{K,w} = \begin{cases} C_1 + O(w^{-0.85}) & \text{for unknots,} \\ C_2 + O(w^{0.85}) & \text{for prime knots,} \\ C_3 + O(w^{1.70}) & \text{for compound knots.} \end{cases} \tag{41}$$

This can be numerically tested.

4 The BFACF algorithm and knotted polygons

Let ω_1 and ω_2 be two knots. These knots are oriented by the addition of a direction along each. Two knots ω_1 and ω_2 are *equivalent* if there is a homeomorphism $F : \mathbb{R}^3 \to \mathbb{R}^3$ such that $F(\omega_1) = \omega_2$. The equivalence classes of (oriented) embeddings of the circle into Euclidean space are called *knot types*. In the case of polygons in $\mathbb{Z}^3$, a knot type is defined as the class of all polygons (viewed as piecewise linear embeddings of the circle in $\mathbb{R}^3$) which are equivalent embeddings in $\mathbb{R}^3$.

A projection P of an embedded circle on any geometric plane $Q \subset \mathbb{R}^3$ is *regular* if (1) there are only a finite number of multiple points in the projection, (2) if all multiple

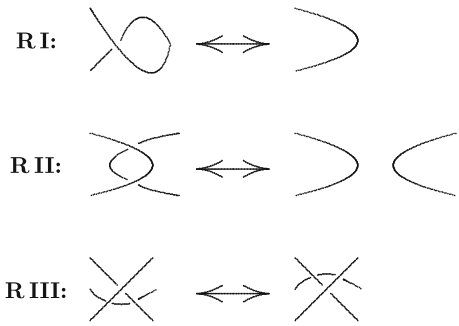

Fig. 9 The Reidemeister Moves. Moves of type I involve a single arc of the knot. Moves of type II involve two arc of the knot, and moves of type III involve three arc of the knot

points are double points where the image of one arc of the knot passes transversely through the image of another arc of the knot, and (3) no vertex of the knot is mapped onto a double point. The projection of a lattice polygon onto a plane Q with irrational direction cosines is always regular.

The knot type of an embedded circle can be determined from a regular projection if at every double point in the projection the overpassing and underpassing strands are indicated together with the orientation. In this case the knot can be reconstructed from its projection. Such a projection is called a *knot projection*.

Reidemeister's theorem states that two knots are equivalent if and only if their regular projections are equivalent under the application of a finite number of Reidemeister moves [33]—these are local operations on the knot projection illustrated in Fig. 9. Thus, if two knots have equivalent knot projections, then they are themselves equivalent. These ideas can be applied to knotted polygons in the cubic lattice.

In what follows, a *subwalk* in a polygon is any sequence of edges in the polygon which constitutes a self-avoiding walk. Let Q be the XY-plane in the cubic lattice, and let ω be a polygon in the cubic lattice. Consider the projection of ω in Q. In general, there will be edges in ω which are parallel to the Z-direction, and these will project to points in Q. Ignore these singular points in the projection.

Apart from these points, in general there will be lattice points in the projection which are at the intersections of projected subwalks in the polygon. These are *multiple points*. There will also be some self-avoiding walks in the projected image which are the projected image of more than one subwalk in the polygon.

Thus, the projection of ω in a lattice plane is in general not regular, even if the singular projections of edges parallel to the Z-axis are ignored.

With these observation, one may define a regular projection for lattice knots.

Definition 4.1 The projection of a lattice knot ω in the XY-plane is said to be *regular* if (1) all multiple points in the projection are double points (the projected images of exactly two vertices in the polygon), if (2) all double points are the images of the two vertices in the polygon where one subwalk of the knot passes transversely over another, if (3) the orientation along the knot is projected onto the lattice projection, and if (4) the projected images of edges parallel to the Z-axis are not considered to be multiple points.

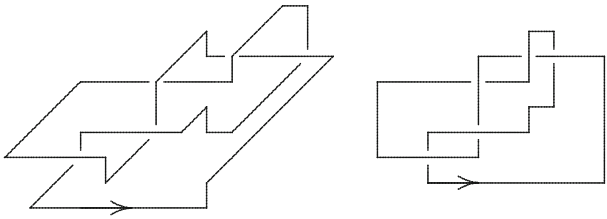

Fig. 10 A regular lattice knot realization of 5_2^+. The projected knot diagram of the knot in the XY-plane is illustrated on the right. This projection is regular in the lattice, and is a lattice knot projection

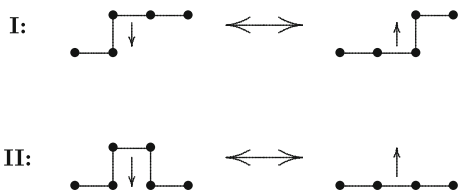

Fig. 11 The BFACF moves operates locally on edges in a polygon; at most five edges is involved in any move. The implementation proceeds by the selection of an edge in the polygon, and then translating it one lattice step in a random direction normal to itself, while deleting or adding edges to preserve the connectivity of the polygon. The results are two different types of moves illustrated above, the first is a length preserving move (I), and the second is a move which may decrease the length of the polygon (II, left to right), or increase the length of the polygon (II, right to left)

Regular projections of lattice knots are *lattice knot projections*. In a w-slab L_w, the projections of lattice knots are in the bottom bounding plane $B(L_w)$ of L_w. In Fig. 10 a lattice knot embedding of the knot 5_2^+, and its lattice knot projection, are illustrated.

4.1 The BFACF algorithm and lattice knots

The BFACF algorithm [1–3] is a Markov Chain Monte Carlo program which samples lattice polygons from a distribution. It was originally used to sample self-avoiding walks with fixed endpoints in the lattice, but has similarly been used to sample lattice polygons. In its standard implementation the algorithm has one parameter t conjugate to the number of edges in the walk or polygon.

The detailed operation of the algorithm on a lattice polygon is based on the two elementary moves displayed in Fig. 11. These may be implemented by choosing an edge uniformly in the walk or polygon, and then translating it normally in one of $2(d-1)$ directions, inserting or deleting edges to keep the polygon connected.

If the polygon becomes longer by two edges in the application of the elementary move, then a Metropolis style implementation [27] would require that it be accepted as the new state in the Markov Chain with probability t^2. If the polygon does not change its length or becomes shorter in the application of the elementary move, then it will be accepted as the new state in the Markov Chain with probability 1.

The above may be modified by choosing the elementary transition probability from a current state ω to an proposed adjacent state ω' to be given by

$$P(\omega \to \omega') = \begin{cases} 1, & \text{if } |\omega'| \leq |\omega|; \\ \left(\frac{|\omega'|^{q-1}}{|\omega|^{q-1}}\right) t^2, & \text{if } |\omega'| = |\omega| + 2, \end{cases} \tag{42}$$

where q is a parameter (see Ref. [31] for details). One may check that the term $\left(|\omega'|^{q-1}/|\omega|^{q-1}\right) t^2$ is always less than 1 for $t \leq 1/\mu$ and $q \leq 3$ (say).

Since the a priori probability to pick a given edge in a polygon ω is $1/|\omega|$, the elementary transition matrix satisfies a detailed balance condition given by

$$|\omega|^q t^{|\omega|}\, p(\omega \to \omega') = |\omega'|^q t^{|\omega'|}\, p(\omega' \to \omega). \tag{43}$$

Within its ergodicity classes K, the algorithm has stationary distribution

$$\Pi_K(\omega) = \frac{|\omega|^q\, t^{|\omega|} \chi_K(\omega)}{\Phi} \tag{44}$$

at activity t, where ω is a polygon. The function χ_K is an indicator function which is 1 if $\omega \in K$ and zero otherwise, and Φ is a normalising constant given by

$$\Phi = \sum_{\omega \in K} |\omega|^q\, t^{|\omega|}. \tag{45}$$

Normally, one would put $q = 0$, but larger values of q will bias the sampling to longer polygons.

In two dimensions it is known that the algorithm is irreducible when applied to both square lattice polygons, and to square lattice walks with fixed endpoints [Madras, 1986 "Unpublished", 26]. Thus, the algorithm is both irreducible and satisfies a condition of detailed balance in two dimensions. In this case the algorithm samples from a unique stationary distribution given by

$$\Pi(w) = \frac{|\omega|^q\, t^{|\omega|}}{\Phi}, \tag{46}$$

where $|\omega|$ is the length of the polygon ω, and Φ is a normalising factor.

The ergodicity properties have also been resolved in three dimensions [11, 17]. In particular, the algorithm is not irreducible for lattice polygons in the cubic lattice. If the algorithm is used to sample polygons along a Markov Chain in three dimensions then it does not have a unique stationary distribution; instead the chain samples from a stationary distribution that depends on the initial state of the Markov Chain. This fixes the ergodicity class of the algorithm for every simulation. The ergodicity classes are described by the following theorem:

Theorem 4.2 *The ergodicity classes of the BFACF algorithm, when applied to unrooted lattice polygons in the cubic lattice, are the knot types of the polygons.*

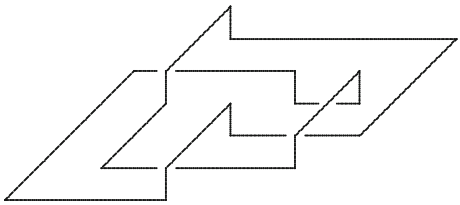

Fig. 12 A realization of the right handed trefoil knot 3_1^+ in L_1

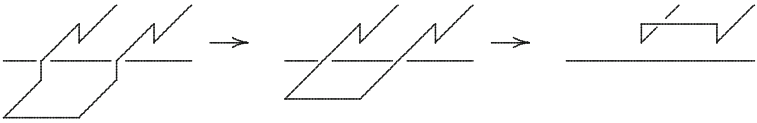

Fig. 13 Performing Reidemeister II in L_1

In other words, the ergodicity classes coincide with the knot-types of lattice polygons. For the proof of this theorem, see Ref. [17], and in particular Theorem 3.11 therein.

In a slab $\mathbb{L}_w$ the ergodicity classes of lattice polygons have similarly been resolved. In the event that $w = 1$, the algorithm does not have ergodicity classes that coincide with knot types of lattice knots in $\mathbb{L}_1$ (see Fig. 12). Instead, the following theorem was proven in Ref. [13]:

Theorem 4.3 *Suppose that ω is a polygon in L_1. Then ω has a regular lattice knot projection in the XY-plane. Moreover, by applying a finite number of BFACF moves in L_1 on ω, Reidemeister moves of type I or of type II can be performed on the lattice knot projection of ω.*

An example of a Reidemeister II move on two arcs in a polygon is given in Fig. 13. To perform Reidemeister III moves on a polygon in $\mathbb{L}_w$, one must have $w > 1$.

Theorem 4.4 *Suppose that ω is a polygon in L_1. Then ω has a regular lattice knot projection in the XY-plane. Moreover, by applying a finite number of BFACF moves in L_2 on ω, Reidemeister moves of type III can be performed on the lattice knot projection of ω.*

The theorems above states that Reidemeister moves can be performed on lattice polygons in three dimensions in $\mathbb{L}_w$, provided that $w > 1$. These results give the following theorem, the methods of proof are directly from proposition 3.9 and proposition 3.10 in Ref. [17]. The result is the following theorem:

Theorem 4.5 *The ergodicity classes of the BFACF algorithm in the set of all unrooted lattice polygons in L_2 are the knot types of the polygons.*

This theorem generalizes to other slabs, with $w > 2$: see Ref. [13].

Theorem 4.6 *Suppose that $w \geq 2$. Then the ergodicity classes of the BFACF algorithm in the set of all unrooted lattice polygons in L_w are the knot types of the polygons.*

There are several open problems which remain unresolved. For example, the ergodicity properties of the BFACF algorithm in $\mathbb{L}_1$ in three dimensions are not understood, and this is posed as an open problem.

Open problem 4.7 *Characterize the ergodicity classes of the BFACF algorithm when it is implemented to three dimensional lattice polygons in the slab* $\mathbb{L}_1$.

In addition, there are no algorithms available for simulating lattice polygons in other confining geometries, such as pores or even in wedges.

Open problem 4.8 *Prove that the BFACF algorithm is ergodic in a cube of dimension w defined by*

$$\mathcal{C}_w = \{\mathbf{x} \in \mathbb{Z}^d \mid 0 \le X(x) \le w, \quad 0 \le Y(x) \le w, \quad 0 \le Z(x) \le w\}.$$

Alternatively, demonstrate that knotted polygons can effectively be sampled in $\mathcal{C}_w$ *by a Monte Carlo algorithm.*

Open problem 4.9 *Prove that the BFACF algorithm is ergodic in a wedge* $\mathcal{W}$ *with vertex angle s defined by*

$$\mathcal{W}_s = \{\mathbf{x} \in \mathbb{Z}^d \mid 0 \le Z(x) \le (\tan s) X(x)\}$$

where the polygon is rooted at the origin $(0, 0, 0)$*, or confined to a finite subset of the wedge.*

The simulation of polygons of fixed length and fixed knot type is a major open problem.

Open problem 4.10 *Construct a Monte Carlo algorithm for the sampling lattice of fixed length in the cubic lattice, or confined in a slab in the cubic lattice.*

4.2 Data analysis

Suppose that the numerical values of an observable $A(\omega)$ are sampled along a time series L generated by sampling along a Markov Chain $\mathcal{M} = \{w_i\}$ using the BFACF algorithm in the state space of the algorithm. Then the sample average of the observable along the chain is

$$\langle\!\langle A \rangle\!\rangle_N = \frac{1}{N} \sum_{i=1}^{N} A(\omega_i) \tag{47}$$

if the chain has length N. Since the chain is ergodic in its ergodicity class K (which coincides with the knot type of the first state ω_1 of the polygons) by theorem 4.6, the sample average of the chain converges to

$$\lim_{N\to\infty} \langle\!\langle A \rangle\!\rangle_N = \frac{1}{\Phi} \sum_{\omega \in K} A(\omega)\, |\omega|^q t^{|\omega|} \tag{48}$$

by the fundamental theorem of Markov Chains where Φ is a normalising factor, and where it is assumed that the Markov Chain is generated by setting the activity parameter of edges equal to t.

The mean value of A measured over a boltzmann distribution is given by

$$\langle A \rangle = \sum_{\omega \in K} A(\omega)\, t^{|\omega|} / \sum_{\omega \in K} t^{|\omega|} \tag{49}$$

and comparison with Eq. 48 shows that the ratio-estimator

$$\langle A \rangle = \frac{\lim_{N\to\infty} \langle\!\langle A/|\omega|^q \rangle\!\rangle_N}{\lim_{N\to\infty} \langle\!\langle 1/|\omega|^q \rangle\!\rangle_N} \approx \frac{\langle\!\langle A/|\omega|^q \rangle\!\rangle_N}{\langle\!\langle 1/|\omega|^q \rangle\!\rangle_N} \tag{50}$$

approximates $\langle A \rangle$ for large values of N.

5 Numerical simulations

The expected length of a polygon in the ensemble defined by Eq. 2, assuming that $p_n \approx A\, n^{\alpha-3}\mu^n$, is given by Eq. 12. Since $\alpha \approx 0.26$, this result clearly shows that $\langle n \rangle \to$ Const. as $t \to t_c = 1/\mu$.

In contrast to this, implementing the BFACF algorithm with the parameter q as defined in the last section gives the stationary distribution 44. For large enough values of q, $\langle\!\langle n \rangle\!\rangle$ will be divergent as $t \to 1/\mu$. In fact, if $p_n(K)$ is given by Eq. 20, with the explicit correction terms

$$p_n(K) = A_K n^{\alpha_K - 3} \mu_K^n \left(1 + B_K n^{-\Delta_K} + C_K n^{-1} + \cdots\right), \tag{51}$$

then it is possible to compute the expected length of polygons in a simulation using the BFACF algorithm, at given fixed values of the parameters t and q. This was done in Ref. [31]. The invariant stationary distribution is given by Eq. 44, and if one assumes that q is large enough to make the mean length of polygons divergent at the critical point $t = 1/\mu$ (it is sufficient to take $q = 3$, for example). Then by taking the derivative of $\log \Phi$ to $\log t$ while taking into account the subdominant corrections to p_n, the mean length of polygons sampled by the algorithm should be given by

$$\begin{aligned}
\langle\!\langle n \rangle\!\rangle_K &\simeq t \frac{-\mu(2-\alpha-q)z^{-1} - \mu(2-\alpha-q)bz^{\Delta} - \mu(2-\alpha-q)c - \mu b\Delta z^{\Delta-1} - \mu c}{1 + bz^{\Delta} + cz} \\
&= \frac{t\mu(\alpha+q-2)}{z}\left\{1 + b\frac{\alpha+q-2-\Delta}{\alpha+q-2}z^{\Delta} + c\frac{\alpha+q-3}{\alpha+q-2}z\right\}\{1 - bz^{\Delta} - cz\} \\
&= \frac{t\mu(\alpha+q-2)}{z}\left\{1 - \frac{\Delta b}{\alpha+q-2}z^{\Delta} + c\frac{\alpha+q-3}{\alpha+q-2}z - bc\frac{2\alpha+2q-5-\Delta}{\alpha+q-2}z^{\Delta+1}\right\}
\end{aligned} \tag{52}$$

where $z = n \ln(\mu t)^{-1}$ and where b and c are only dependent on q. Keeping only the leading terms, and fixing the knot type at K, then shows that

$$\langle\!\langle n \rangle\!\rangle_K \approx \frac{[\alpha_K + q - 2]\mu_K t}{1 - t\mu_K} \left(1 - \frac{B_K \Delta_K [1 - t\mu_K]^{\Delta_K}}{\alpha_K + q - 2}\right). \tag{53}$$

Taking ratios for two different knot types show (assuming that Δ is independent of knot type)

$$\frac{\langle\!\langle n \rangle\!\rangle_K}{\langle\!\langle n \rangle\!\rangle_L} \approx \frac{\alpha_K + q - 2}{\alpha_L + q - 2} \left[1 + c(1 - t\mu(\emptyset))^{\Delta}\right]. \tag{54}$$

In simulations with $q = 3$, define

$$\rho(K, L) = \frac{\alpha_K + 1}{\alpha_L + 1}. \tag{55}$$

Computing $\rho(K, L)$ is a numerical verification of the relation $\alpha_K = \alpha_\emptyset + N_K$ in Eq. 21.

5.1 The growth constant

Plots of $\langle n \rangle_K^{-1}$ as a function of $1/t$ have been made for data obtained with $q = 3$ for some simple knots in Ref. [31]. For t close to its critical value $(1/\mu_K)$, linear behaviour of the data can be extrapolated to estimate the growth constant μ_K. This procedure gave the following estimates

$$\begin{aligned} \mu_\emptyset &= 4.6852, \\ \mu_{3_1} &= 4.6832, \\ \mu_{4_1} &= 4.6833, \\ \mu_{6_2} &= 4.6844, \\ \mu_{3_1 \# 3_1} &= 4.6800, \\ \mu_{3_1 \# 4_1} &= 4.6841. \end{aligned} \tag{56}$$

These values coincide to the second decimal place, and it seems reasonable to take this as evidence that they are all equal: $\mu_\emptyset = \mu_K$ for any knot type K. This result is consistent with Open problem 2.3. Since these results were independently obtained, their average can be taken to estimate the growth constant for polygons of fixed knot type:

$$\mu_\emptyset = \mu_K = 4.6836 \pm 0.0038, \quad \text{(95\% confidence interval) for any knot type } K. \tag{57}$$

Current computer technology should be powerful enough to determine more digits in $\mu_\emptyset$, and to compare them with Eq. 7 to verify the estimate in Eq. 17. This is an open problem.

Open problem 5.1 *Compute $\mu_\emptyset$ and μ_{3_1} to higher accuracy in order to demonstrate numerically that*

$$\log \mu_{3_1} - \log \mu_{0_1} = 0.$$

5.2 The entropic exponent

Estimates of $\rho(K, L)$ were also made in Ref. [31] (see also Ref. [29]). If $\alpha_K = \alpha_L$, then $\rho(K, L) = 1$. Otherwise, assuming that $\alpha_\emptyset = 0.237 \pm 0.004$ (which is the numerical value for polygons [22]), one should obtain $\rho(K, \emptyset) \approx 1.80$ if K is prime, and $\rho(K, P) \approx 1.44$ if K is compound with two components and P is a prime knot.

In Ref. [31] the following measurements were made:

$$\begin{aligned} \rho(3_1, \emptyset) &= 1.69 \pm 0.11, \\ \rho(4_1, \emptyset) &= 1.67 \pm 0.11, \\ \rho(6_2, \emptyset) &= 1.75 \pm 0.05. \end{aligned} \tag{58}$$

and moreover,

$$\begin{aligned} \rho(3_1, 4_1) &= 1.01 \pm 0.11, \\ \rho(3_1\#3_1, 3_1\#4_1) &= 0.928 \pm 0.070. \end{aligned} \tag{59}$$

In the case of 3_1 and 4_1,

$$\begin{aligned} \rho(3_1\#3_1, 3_1) &= 1.25 \pm 0.16, \\ \rho(3_1\#3_1, 4_1) &= 1.38 \pm 0.06, \\ \rho(3_1\#4_1, 3_1) &= 1.27 \pm 0.02, \\ \rho(3_1\#4_1, 4_1) &= 1.39 \pm 0.10. \end{aligned} \tag{60}$$

These results strongly support the notion that $\alpha_K = \alpha_\emptyset + N_K$. This relation can be understood by arguing as in Sect. 5.2.1 using the metric scaling of a polygon of knot type K.

Open problem 5.2 *improve the accuracy of the results above to demonstrate numerically to better accuracy that $\alpha_K = \alpha_\emptyset + N_K$.*

5.2.1 The metric exponent

The mean square radius of gyration of a polygon of knot type K must grow as a powerlaw of n

$$\langle R^2 \rangle_K \approx M_K n^{2\nu_K} \tag{61}$$

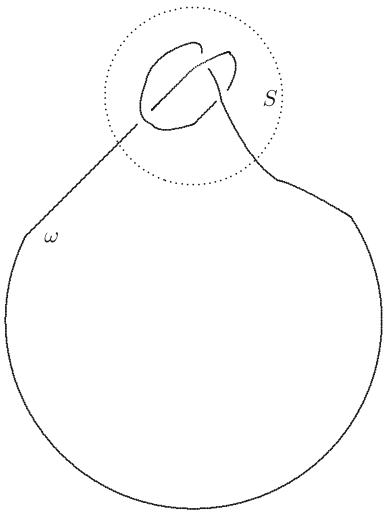

Fig. 14 A schematic diagram of a knotted arc in a ball in polygon. The ball separates the knotted polygon into two arcs, one which is knotted if it is closed by an arc on the ball

where ν_K is the metric exponent, and M_K is an amplitude, and where $1/3 \leq \nu_K \leq 1$. Numerical simulations strongly suggest that both ν_K and M_K are independent of K [18].

Open problem 5.3 *Show numerically or otherwise that $\nu_K = \nu_\emptyset = \nu$, where ν is the metric exponent of the self-avoiding walk in three dimensions. In addition, demonstrate that the amplitude M_K in Eq. 61 is independent of K to higher accuracy than was done in Ref. [18].*

Figure 14 is a schematic diagram of a polygon ω which is a prime knot. Let S be a geometric sphere which intersects ω in exactly two points. Then S divides ω into two arcs, each of which can be closed by a shortest curve on the sphere into an embedded circle. One of these arcs, closed by a curve on S, is a knot. Let its length be m_K, assuming that ω has n edges.

Define M_K to be the infimum of m_K over all possible intersections of geometric spheres which cut ω in exactly two points. Define n_K to be the expected value of M_K taken uniformly over all polygons of knot type K.

There are two possibilities: First of all, one may have $n_K \propto n$ (assume that $n_K/n \to \gamma$ for some constant γ), or alternatively, $n_K = o(n)$.

If $n_K \propto n$, then the mean length of the arc of ω inside S grows, on average, proportionally to n, and the radius of S grows at least as fast as $O(n^{1/3})$, and at most as $O(n^\nu)$. If $\langle R_n^2 \rangle_K^{1/2}$ grows faster than the radius of S, then ω will start to assume the character of an unknotted polygon of length $(1-\gamma)n$, and observe then that $\nu_\emptyset = \nu_K$, while $M_K = (1-\gamma)M_\emptyset < M_\emptyset$.

If $\langle R_n^2 \rangle_K^{1/2}$ grows at the same rate as the radius of S (this may be the case if $\gamma = 1$) then it is not possible to derive a relationship between the critical exponents or amplitudes.

On the other hand, if one consider the case that $n_K = o(n)$, then $\nu_K = \nu_\emptyset$ by the same arguments as in the case above. In addition, the scaling of the mean square radius

of gyration now has the general form

$$\langle R_n^2 \rangle_K \approx M_K (n - n_K)^{2\nu_\emptyset} \approx M_\emptyset n^{2\nu_\emptyset} (1 + \lambda n_K / n + \cdots), \tag{62}$$

for some constants M_K and λ. Thus, if $n_K = o(n)$, then the knot has no effect on the amplitude (M_K is independent of the knot type) and the effect of the knot only appears as corrections to the scaling. For example, if $n_K \sim \sqrt{n}$, then a correction term of the form $\lambda/\sqrt{n}$ will appear, and so on. Numerical evidence indicates that M_K is independent of K [17]. Overall, this argument strongly support the notion that $\nu_\emptyset = \nu_K$ for arbitrary knot types K.

These arguments also have implications for the entropic exponent: Indeed, if $n_K = o(n)$, then in the large n limit, the knotted polygon looks like an unknotted polygon with a small sphere attached to it, and where its knot type is determined. Since we can place this sphere and its contents at $O(n)$ places along the polygon, we conclude that $p_n(K) \sim n\, p_n(\emptyset)$. Substitution of Eq. (20) gives $\alpha_K = \alpha_\emptyset + 1$, if K is a prime knot. This argument generalises to cases where K is a knot with N_K prime components, and suggests that $\alpha_K = \alpha_\emptyset + N_K$.

5.3 The mean length of knotted polygons in slabs

The mean length of a knotted polygon in a w-slab should increase with w as in Eqs. 40 or 41 at activity $t = \mu_\emptyset^{-1}$, where $\mu_\emptyset^{-1}$ is the growth constant of unknotted polygons in the cubic lattice.

In the case of unknotted polygons one may approximate $\alpha_\emptyset = \alpha = 1/2$ and $\alpha/\nu = 0.85$ in Eq. 40 to obtain

$$\langle n \rangle_w = C_1 + C_2\, w^{-0.85} + \cdots \tag{63}$$

Thus, the mean length of unknotted polygons should approach a constant as $w \to \infty$. Moreover, the approach should be at a rate proportional to $w^{-0.85}$. Since unknotted polygons are believed to have the same scaling exponents as all polygons, this behaviour should also be true for all polygons in a w-slab.

In Fig. 15 the increase in the mean length of unknotted polygons with w is plotted for values of $w \in [1, 22]$. A best fit is indicated by the solid line. The χ^2-statistics of this regression was acceptable at the 95% level on the points spanned by the solid curve. The regression estimates that $C_1 = 7.248 \pm 0.007$ in Eq. 63.

In the case of knotted polygons of prime knot type one may approximate $\alpha_K = \alpha_\emptyset + 1$ with the result that the mean length diverges with w. From Eq. 40 one obtains

$$\langle n \rangle_w = C_1 + C_2\, w^{0.85} + \cdots \tag{64}$$

The mean length of polygons with knot type 3_1 (trefoil) is plotted in Fig. 16 at $t = \mu_\emptyset^{-1}$. In contrast with unknotted polygons, the mean length of trefoils increases quickly with w. Although the graph may appear linear for $w > 4$, a least squares regression using the model $\langle n \rangle_w = C_1 + C_2\, w^{0.85} + C_3/w$ was used (see Eq. 64). The solid lines span

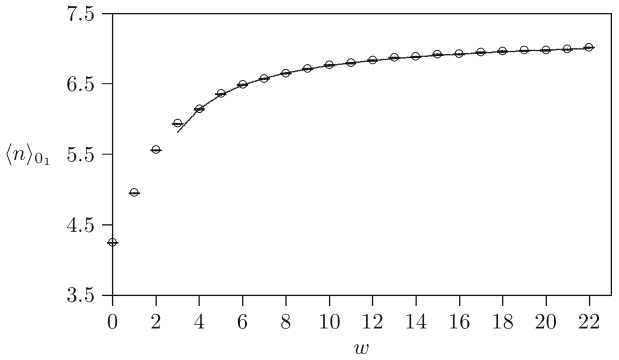

Fig. 15 The mean length $\langle n \rangle_{0_1}$ of unknotted polygons in a slab of width w at $t = 1/\mu_\emptyset$. This data have been fitted with the model $C_1 + C_2\, w^{-0.85} + C_3/w$ (compare this to Eq. 41). Extrapolating suggests that the curve is asymptotic to the constant 7.248 ± 0.007

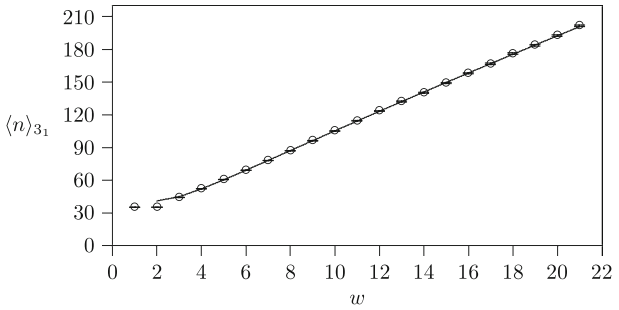

Fig. 16 The mean length $\langle n \rangle_{3_1}$ of polygons knotted into trefoils in a slab of width w at $t = 1/\mu_\emptyset$. This data have been fitted with the model $C_1 + C_2\, w^{0.85} + C_3/w$ (compare this to Eq. 41). Notice the difference in scale on the vertical axis when compared to Fig. 15

the data points on which a regression acceptable at the 95% level was obtained. These data are consistent with the model, but measurements at larger values of w will be needed to rule out a linear relationship between $\langle n \rangle_w$ and w for trefoils.

Open problem 5.4 *Show numerically that the data in Fig. 16 lie along a concave curve.*

Mean lengths were also computed for other prime knots, and the results are plotted in Fig. 17, displaying data for prime knots up to six crossings in the standard knot tables. In each case the data were fitted assuming the model in Eq. 64; a least squares regression using the model $\langle n \rangle_w = C_1 + C_2\, w^{0.85} + C_3/w$ was used. The solid lines span the data points on which a regression acceptable at the 95% level was obtained. For the knots in this example, the data fall into clear groups defined by minimal crossover number. This is unlikely to persist for more complicated knots.

Compound knots of the form $3_1^+ \# 3_1^+$ and $3_1^+ \# 3_1^+ \# 3_1^+$ (where each copy of 3_1 is right-handed) where also studied. These data, together with data for 3_1, are plotted in

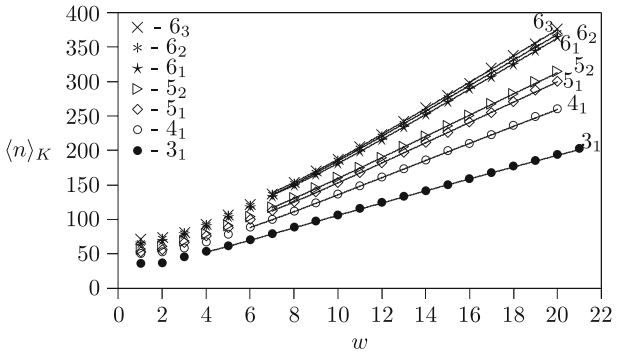

Fig. 17 The mean length $\langle n \rangle_K$ of polygons knotted into prime knots in a slab of width w at $t = 1/\mu_\emptyset$. This data have been fitted with the model $C_1 + C_2\, w^{0.85} + C_3/w$ (compare this to Eq. 41). Notice the difference in scale on the vertical axis when compared to figure 15

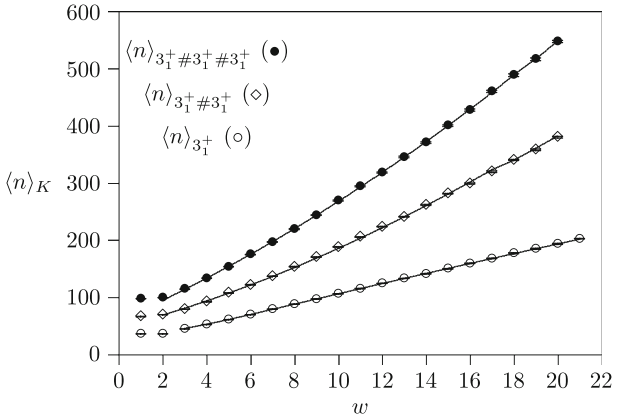

Fig. 18 The mean length $\langle n \rangle_K$ of polygons knotted into compound knots and for the trefoil knot in a slab of width w at $t = 1/\mu_\emptyset$. This data have been fitted with the model $C_1 + C_2\, w^{1.85} + C_3/w$ (compare this to Eq. 41). Notice the difference in scale on the vertical axis when compared to Figs. 15 and 17

Fig. 18. In the case of compound knots, the data is modeled by

$$\langle n \rangle_w = C_1 + C_2\, w^{1.85} + \cdots \tag{65}$$

as suggested in Eq. 40. Thus, a least squares regression using the model $\langle n \rangle_w = C_1 + C_2\, w^{1.85} + C_3/w$ was used to fit the data. The solid lines span the data points on which a regression acceptable at the 95% level was obtained. The data for 3_1 are reproduced from Fig. 17.

The predicted behaviour from Eq. 64 is that the mean length will increase along a concave curve with increasing w for prime knots other than the unknot, while the mean length will increase along a convex curve with increasing w for compound knots. This is supported by the data in Fig. 18; there is a clear convexity in the data for the compound knots. However, for the prime knots in Figs. 17 and 18, larger values of w

may be needed to confirm that the data lie along a concave curves—these calculations are computationally expensive.

5.4 Metric properties of knotted polygons in a slab

In this section the metric properties of knotted polygons in a slab are discussed. In particular, data were collected using the BFACF algorithm in a slab geometry, and analysed in Ref. [13]. Those data have been used to generate Figs. 19, 20 and 21.

In Fig. 19 the mean square radius of gyration of knotted polygons in a w-slab are plotted against w for the unknot, the trefoil and for composite trefoil knot types. Unknotted polygons stay on average small with increasing w. In fact, unknotted poly-

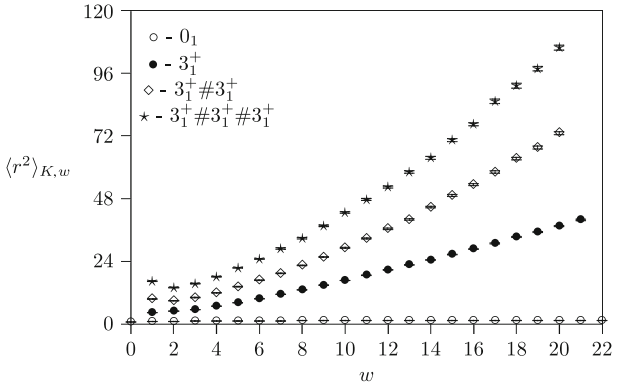

Fig. 19 The mean square radius of gyration of lattice polygons with knot type compounded trefoils. Increasing w increases the mean length of the polygons, and they grow in relative size. The more complex knots is swollen in the XY-plane, and so has larger mean square radius of gyration

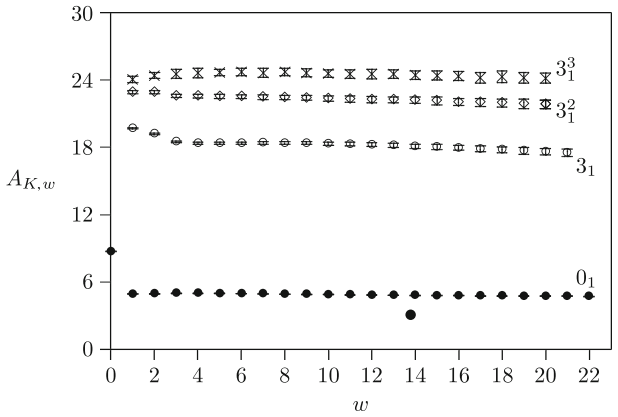

Fig. 20 Amplitude ratios of polygons with knot type compounded trefiols. The data show a constant regime for $3 \leq w \leq 10$, before the interactions between the polygon and the slab lessens, and the relative expansion of the polygon becomes less in the XY-plane

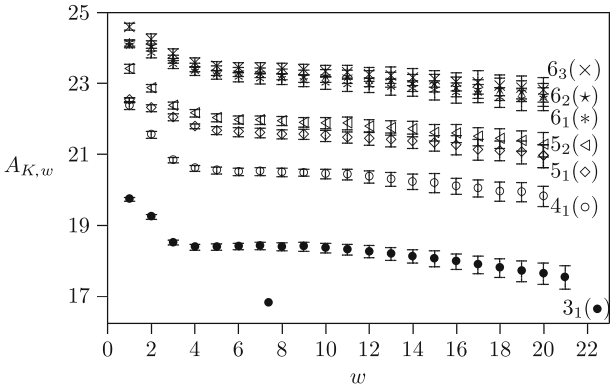

Fig. 21 Amplitude ratios of polygons with prime knot type. The data show a constant regime for $3 \leq w \leq 10$, before the interactions between the polygon and the slab lessens, and the relative expansion of the polygon becomes less in the XY-plane

gons have mean square radius of gyration much smaller than w for even small values of w, an they do not interact significantly with the bounding planes of the slab.

This situation changes for non-trivial knot types. In the case of trefoils (denoted by $\bullet$ in Fig. 19), there is a commensurate increase of $\langle r^2 \rangle_{K,w}$ with w. Our data generally only include values of w up to $w = 20$; extrapolation of the data suggest that this increase is unbounded with w: Increasing w to infinity would also take the mean square radius of gyration of the knotted polygon to infinity. Thus, polygons of non-trivial knot type interact with the bounding planes of the slab, even in the large w limit.

In Fig. 19 data corresponding to the compound knot types $3_1^+ \# 3_1^+$ and $3_1^+ \# 3_1^+ \# 3_1^+$ are denoted by $\diamond$ and $\star$ respectively. The increase in $\langle r^2 \rangle_{K,w}$ is even faster for these knot types than for polygons with knot type a trefoil. The faster expansion of the mean square radius of gyration for composite knots is explained by noting that these polygons expand faster in the XY-direction than a polygon with knot type a trefoil.

One may compute a dimensionless amplitude ratio by taking the ratio of the square of the mean span of a knotted polygon in the XY-plane by the mean square radius of gyration of the polygon: Let $\langle S_{xy} \rangle_{K,w}$ be the mean span of the knotted polygon in the XY-plane and define the amplitude ratio $A_{K,w}$ by

$$A_{K,w} = \frac{\langle S_{xy} \rangle_{K,w}^2}{\langle r^2 \rangle_{K,w}}. \tag{66}$$

$A_{K,w}$ is generally a function of the activity t, and in Fig. 20 it is plotted at $t = \mu_{\emptyset}^{-1}$ for the unknot and for trefoils and compound trefoils.

The amplitude ratios in Fig. 20 are virtually independent of w for unknotted polygons. This shows that unknotted polygons can be accommodated in a w-slab without the polygon spreading out in the XY-direction to compensate for the steric repulsions between subwalks of the polygon induced by the w-slab.

For knotted polygons however, closer inspection shows that $A_{K,w}$ goes through a constant regime for w roughly in the range $4 \leq w \leq 10$, before it starts to decline slowly in value for larger values of w. The constant regime appears to be the result of steric interactions between subwalks in the knot induced by the slab. The smallest geometric sphere intersecting the polygon in two points, and which contains an arc in the polygon which closes to a knot along the surface of the sphere will be comparable in size to the polygon itself for small values of w, and this sphere should grow in size proportional to the span in the XY-plane. For larger values of w the size of the knotted ball-pair reduces relative to the size of the polygon, and eventually it stops interacting with the bounding planes; hence the decline that sets in the amplitude ratios in Fig. 14 for larger values of w.

The data in Fig. 20 may be interpreted as follows: At smaller values of w the knot spreads out in the XY-direction proportional to its mean square radius of gyration, giving rise to the observed constant regime. This constant plato in $A_{K,w}$ is a measure of the amount of spreading of the knot in the XY-direction due to its complexity. The more "complex" a knot, the more it should spread out in the XY-direction for narrow w-slabs, and the larger $A_{K,w}$ should be in its constant regime. The average value of $A_{K,w}$ in this constant regime is a measure of complexity of the knot.

For larger values of w the knotted ball-pair can be accommodated in the slab, and the expansion of the polygon in the XY-plane is less.

Observe also that in Fig. 20 $A_{K,w}$ increases with K going from the unknot to a knot which is the connected sum of three right handed trefoils.

In Table 1 the average of the amplitude ratios

$$\langle A_{K,w} \rangle = \frac{1}{7} \sum_{w=4}^{10} A_{K,w} \tag{67}$$

for values of w from 4 to 10 are listed. This range of w is over the constant regime in Figs. 20 and 21. These estimates of the mean amplitude ratio give a measurement of the deformation of the knot in slabs where steric interactions in the polygon as a result

Table 1 The Average of $A_{K,w}$ for $4 \leq w \leq 10$

Knot	$A_{K,4}$	$A_{K,10}$	$\langle A_{K,w} \rangle$ Eqn. 67
0_1	4.952(21)	4.834(19)	4.90
3_1	18.499(69)	18.343(138)	18.38
4_1	20.599(85)	20.438(141)	20.51
5_1	21.781(71)	21.519(155)	21.61
5_2	22.156(106)	21.872(161)	21.97
6_1	23.342(119)	23.003(171)	23.15
6_2	23.446(122)	23.209(176)	23.30
6_3	23.589(128)	23.352(164)	23.45
$3_1^+ \# 3_1^+$	22.588(156)	23.377(230)	22.50
$3_1^+ \# 3_1^-$	22.565(149)	22.368(232)	22.50
$3_1^+ \# 3_1^+ \# 3_1^+$	24.645(429)	24.619(223)	24.68

of the knot type expands the knot in the XY-plane. The second and third columns in Table 1 lists the values of $A_{K,w}$ for $w = 4$ and $w = 10$ respectively. These values are largely unchanged for this range of w.

Similar observations are true when only prime knot types are considered. $A_{K,w}$ are plotted against w in Fig. 21 for K ranging over knots from 3_1 to 6_3 in the standard knot tables. The vertical scale in Fig. 21 has been stretched to enhance changes in the vertical direction, and the constant regimes in $A_{K,w}$ are quite visible in this plot, ranging for w between 4 and roughly 10 for each knot type.

The metric properties of the knotted polygons were examined in Figs. 19, 20 and 21. In Fig. 19 it was found that the mean square radius of gyration increases with w for non-trivial knots. This is not unexpected, since the length of polygons with non-trivial knot types increases with w. The amplitude ratios do however tell a more interesting story.

The amplitude ratios defined in Eq. 66 may be interpreted as a measure of the deformation of the polygon by the slab. A larger value of $A_{K,w}$ implies that the polygon is expanded in the XY-directions parallel to the slab, while a smaller amplitude ratio is consistent with a polygon that on average is not deformed significantly by the confining geometry of the slab.

If $A_{K,w}$ decreases with w, then the entanglements in the knot are increasingly accommodated by the w-slab, and the deformation of the polygon by the slab is lessened.

In narrow slabs the entanglements in the polygon are compensated for by a relative expansion of the knot in the XY-direction. This shows that more complex knots with more steric repulsions due to entanglements should have an increased amplitude ratio, as observed numerically in Figs. 20 and 21.

The constant regimes in Figs. 20 and 21 are regimes where the square of the XY-span and the mean square radius of gyration increase at a similar rate with w. This increase is probably proportional to w. This implies that the deformation of the knot by the slab does not change with increasing w, because the polygon must accommodate entanglements in the knot by expanding in the XY-direction.

As the entanglements in the knot are relaxed by an increasing w, the knot grows in all directions at a similar rate until the polygon reaches a length where it can accommodate the knot without losing significant entropy or by interacting with the slab. At this point the entanglements due to the knot type become less a factor in its overall mean shape, and the polygon need not expand in the XY-direction to compensate. This implies a smaller XY-span relative to the mean square radius of gyration. This implies that $A_{K,w}$ should decrease with w, and this is observed in Figs. 20 and 21.

6 Conclusions

In this paper an review of the status of lattice knot statistics is given. This review is by no means comprehensive, and focussed in particular on the statistics of lattice knots in slabs. Open problems in the study of lattice knots were proposed, some of which would be key results if they are resolved. Perhaps the most important open questions

are stated in Open problems 2.2 and 2.3, and 2.4. Proving (or disproving!) these results will put on firmer basis much of what is assumed in the rest of this review.

The study of knotted polygons in confined geometries here focus on the one example of a knotted polygon in the cubic lattice confined to a slab. Monte Carlo simulations of this situation are possible because the BFACF algorithm can be shown to be ergodic in slabs in the cubic lattice; this is by no means inevitable, and proving it for other situations remains beyond the scope of current techniques.

The response of knotted polygons confined to a slab were studied in this paper. Scaling arguments were used to predict the mean length of a polygon of fixed knot type and with edges weighted by the activity t. When $t = t_c = \mu^{-1}$, the mean length is given by Eq. 12 and this relation should also apply for knotted polygons, but with μ replaced by $\mu_\emptyset$.

In Sect. 3 it was proven that the BFACF algorithm can be used to similate knotted polygons of fixed knot types in a w-slab. The algorithm is ergodic in the w-slab if $w \geq 2$, but the properties of the algorithm are not yet understood in the 1-slab. The 0-slab is the square lattice, and here it is known that the algorithm is ergodic for unknotted polygons (Madras, 1986 "Unpublished"). Data were collected on realizations of Markov Chains for polygons of fixed knot type in w-slabs for $2 \leq w \leq 20$, with $w = 21$ also included for the trefoil knot, and $w = 21$ and $w = 22$ also included for the unknot.

In Sect. 5 the mean length of knotted polygons and the metric properties of the knotted polygons were examined. In Figs. 15, 16, 17 and 18 the mean length $\langle n \rangle_{K,w}$ are plotted against w. The results in these graphs are consistent with the predicted scaling behaviour in Eq. 39. A particularly interesting point is that the dependence of $\langle n \rangle_{K,w}$ on w is a concave curve for the unknot and prime knots while it is predicted to be convex for composite knots, and this is also observed in Fig. 11. In addition, the mean length of unknotted polygons $\langle n \rangle_{0_1,w}$ approaches a constant as w increases; this is predicted in Eq. 41 and observed in Fig. 9. For all non-trivial knots, $\langle n \rangle_{K,w}$ increases without bound as w increases.

Acknowledgement E.J. Janse van Rensburg is grateful for financial support from NSERC (Canada) in the form of an operating grant.

References

1. C. Aragão de Carvalho, S. Caracciolo, Phys. Rev. B **27**, 1635–1645 (1983)
2. C. Aragão de Carvalho, S. Caracciolo, J. Fröhlich, Nucl. Phys. B **215**(FS7), 209–248 (1983)
3. B. Berg, D. Foester, Random paths and random surfaces on a digital computer. Phys. Lett. **106B**, 323–326 (1981)
4. N. Clisby, R. Liang, G. Slade, Preprint (2007)
5. P.G. de Gennes, *Scaling Concepts in Polymer Physics* (Cornell University Press, Ithaca, 1979)
6. M. Delbruck, Proc. Symp. Appl. Math. **14**, 55–63 (1962)
7. H.L. Frisch, E. Wasserman, J. Amer. Chem. Soc. **83**, 3789–3795 (1961)
8. J.M. Hammersley, Math. Proc. Camb. Phil. Soc. **58**, 235–238 (1961)
9. J.M. Hammersley, K.W. Morton, J. Roy. Stat.l Soc. **B16**, 76–79 (1954)
10. T. Hara, G. Slade, Rev. Math. Phys. **4**, 235–327 (1990)
11. E.J. Janse van Rensburg, J. Phys. A Math. Gen. **25**, 1031–1042 (1992)

12. E.J. Janse van Rensburg, *The Statistical Mechanics of Interacting Walks, Polygons, Animals and Vesicles. Oxford Lect. Ser. Math. Appl.*, vol. 18 (Oxford University Press, Oxford, 2000)
13. E.J. Janse van Rensburg, J. Stat. Mech. Theo. Exper. **03**, P03001 (2007)
14. E.J. Janse van Rensburg, E. Orlandini, D.W. Sumners, M.C. Tesi, S.G. Whittington, J. Knot Theo. Ram. **6**, 31–44 (1996)
15. E.J. Janse van Rensburg, E. Orlandini, S.G. Whittington, J. Phys. A Math. Gen. **39**, 13869–13902 (2006)
16. E.J. Janse van Rensburg, S.G. Whittington, J. Phys. A Math. Gen. **23**, 3573–3590 (1990)
17. E.J. Janse van Rensburg, S.G. Whittington, J. Phys. A Math. Gen. **24**, 5553–5567 (1991)
18. E.J. Janse van Rensburg, S.G. Whittington, J. Phys. A Math. Gen. **24**, 3935–3948 (1991)
19. I. Jensen, J. Phys. A Math. Gen. **36**, 5731–5745 (2003)
20. H. Kesten, J. Math. Phys. **4**, 960–969 (1963)
21. H. Kesten, J. Math. Phys. **5**, 1128–1137(1964)
22. B. Li, N. Madras, A.D. Sokal, J. Stat. Phys. **80**, 661–754 (1995)
23. N. Madras, in *Random Walks, Brownian Motion and Interacting Particle Systems*, ed. by R. Durrett, H. Kesten (Birkhauser, Boston, 1991)
24. N. Madras, J. Stat. Phys. **78**, 681–699 (1995)
25. N. Madras, G. Slade, *The Self-avoiding Walk* (Birkhäuser, Boston, 1993)
26. N. Madras, A.D. Sokal, J. Stat. Phys. **47**, 573–595 (1987)
27. M. Metropolis, A.W. Rosenbluth, M.N. Rosenbluth, A.H. Teller, E. Teller, J. Chem. Phys. **23**, 1087–1092 (1953)
28. B. Nienhuis, Phys. Rev. Lett. **49**, 1062–1065 (1982)
29. E. Orlandini, M.C. Tesi, E.J. Janse van Rensburg, S.G. Whittington, J. Phys. A Math. Gen. **29**, L299–303 (1996)
30. E. Orlandini, M.C. Tesi, E.J. Janse van Rensburg, S.G. Whittington, J. Phys. A Math. Gen. **30**, L693–698 (1997)
31. E. Orlandini, M.C. Tesi, E.J. Janse van Rensburg, S.G. Whittington, J. Phys. A Math. Gen. **31**, 5953–5967 (1998)
32. N. Pippenger, Disc. Appl. Math. **25**, 273–278 (1989)
33. K. Reidemeister, *Knotentheorie* (Springer, Berlin, 1932)
34. C.E. Soteros, D.W. Sumners, S.G. Whittington, Math. Proc. Camb. Phil. Soc. **111**, 75–91 (1992)
35. C.E. Soteros, S.G. Whittington, J. Phys. A Math. Gen. **21**, L857–861 (1988)
36. D.W. Sumners, S.G. Whittington, J. Phys. A Math. Gen. **21**, 1689–1694 (1988)
37. M.C. Tesi, E.J. Janse van Rensburg, E. Orlandini, S.G. Whittington, J. Phys. A Math. Gen. **30**, 5179–5194 (1997)
38. S.G. Whittington, E.J. Janse van Rensburg, Math. Mod. Sci. Comp. **2**, 741–746 (1992) Proc. Eighth Int. Conf. Math. Comp. Mod.
39. S.G. Whittington, C.E. Soteros, Isreal J. Chem. **31**, 127–133 (1991)
40. S.G. Whittington, C.E. Soteros, Macromol. Rep. A **29**(Suppl. 2), 195–199 (1992)